

Analytical method for computing the covariance matrix of cosmic shear two-point correlation function

Kosuke Nagura,^{a,b} Ryo Terasawa,^{c,a} Taisei Terawaki,^{a,b}
Masahiro Takada,^{a,d}

^aKavli Institute for the Physics and Mathematics of the Universe (WPI), The University of Tokyo Institutes for Advanced Study (UTIAS), The University of Tokyo, 5-1-5 Kashiwanoha, Kashiwa-shi, Chiba, 277-8583, Japan

^bDepartment of Physics, The University of Tokyo, Bunkyo, Tokyo 113-0031, Japan

^cCenter for Frontier Science, Chiba University, 1-33 Yayoi-cho, Inage-ku, Chiba 263-8522, Japan

^dCenter for Data-Driven Discovery (CD3), Kavli IPMU (WPI), UTIAS, The University of Tokyo, Kashiwa, Chiba 277-8583, Japan

E-mail: kosuke.nagura@ipmu.jp, ryo.terasawa@chiba-u.jp, taisei.terawaki@ipmu.jp,
masahiro.takada@ipmu.jp

Abstract.

Accurate estimation of the covariance matrix of cosmic shear statistics is essential for cosmological analyses using current and upcoming wide-area weak lensing surveys. In this work, we investigate analytical methods for computing the Gaussian covariance matrix of the cosmic shear two-point correlation function (2PCF), taking into account the effects of finite survey geometry. We compute the covariance of 2PCF based on the improved Narrow Kernel Approximation (iNKA), with a projection using the Legendre transformation. We also consider other analytical covariance estimators, the f_{sky} approximation and the weighted quartic-counts method. We evaluate the accuracy of those analytical methods using the convergence fields with the HSC Year 3 survey mask as a test case. We find that the covariance of the 2PCF obtained by using the iNKA does not reproduce the covariance measured directly from Gaussian simulations. Although the iNKA accurately models the diagonal structure of the harmonic-space covariance, residual inaccuracies in the off-diagonal components propagate through the Legendre transformation and significantly affect the real-space covariance. In contrast, the weighted quartic-counts method shows better agreement with the simulations. Our results demonstrate that accurate modeling of the off-diagonal structure of the harmonic-space covariance is crucial for obtaining reliable covariance estimates of real-space weak lensing statistics in the presence of survey window effects.

Contents

| | | |
|----------|--|----------|
| 1 | Introduction | 1 |
| 2 | Formulation of the covariance matrix of cosmic shear two-point correlation function | 2 |
| 2.1 | Power spectrum with and without survey window effects | 2 |
| 2.2 | Relation between $\xi(\theta)$ and \tilde{C}_ℓ | 3 |
| 2.3 | Covariance matrix of $\xi(\theta)$ | 3 |
| 2.3.1 | Improved Narrow Kernel Approximation (iNKA) | 4 |
| 2.3.2 | The f_{sky} approximation | 4 |
| 3 | Gaussian simulations of cosmic shear fields | 4 |
| 3.1 | Cosmological parameters and simulation setups | 4 |
| 3.2 | Measurements of \tilde{C}_ℓ , $\xi(\theta)$, and their covariance matrices from simulated maps | 5 |
| 4 | Results | 5 |
| 4.1 | Signal of \tilde{C}_ℓ , $\xi(\theta)$ | 5 |
| 4.2 | Covariance of $\xi(\theta)$ | 6 |
| 4.3 | 2PCF covariance from quartic counts | 8 |
| 5 | Conclusion | 9 |

1 Introduction

Current photometric surveys have given a wealth of information on the structure formation. When performing the cosmology analysis of such data, it is important to estimate the covariance accurately. In this work, we focus on the covariance of angular two-point correlation functions (2PCFs) and angular power spectrum, which are widely used in the literature. Roughly speaking, there are two ways to compute the covariance: to measure sample covariance from the many simulation realizations, or to model the covariance analytically.

The former one is used in the Hyper Suprime-Cam (HSC) analyses (e.g., [1–5]). By cutting out the survey region from full-sky simulations [6], we can take into account for the effect of the survey geometry including the Super-Sample Covariance (SSC) (e.g., [7–9]). Being made off of N-body simulations, covariance from the full-sky simulations incorporate non-Gaussian Covariance which arise from connected trispectrum. For the surveys with relatively small sky area such as HSC, we can cut out multiple pseudo-independent realizations from one full-sky simulation, but for the Stage-IV surveys with area $\gtrsim 10,000 \text{ deg}^2$, only few realizations can be extracted from a full-sky simulation and making many full-sky simulations will be computationally expensive.

To circumvent the expensive simulations, modeling covariance analytically (e.g., [10–18]) would be realistic option for the Stage-IV surveys. In the analytic model, the covariance is calculated as a sum of Gaussian Covariance term and non-Gaussian Covariance term. In this work, we focus on the Gaussian term which is dominant on the large scales. In the upcoming survey with wide area, the large-scale data becomes important [19, 20] and so is its covariance.

Survey masks introduce mode-coupling and affect covariance. The Gaussian Covariance for pseudo- C_ℓ estimator in the presence of mask is studied in Refs [21–23]. For the two-point correlation functions, the effect of window can be taken into account by accurately calculating number of pairs of galaxies in angular bin for the shot/shape noise term [24]. For the mixed contributions from the sample variance and shot/shape noise (“mixed term”), triplet counting gives accurate estimate [12]. For the sample variance-only term, corresponding calculation involves with quartic counts [13, 25] which can be computationally expensive. Hence, in this paper, focusing on the sample variance-only term, we explore the other approach where the real-space covariance is calculated as a double Legendre transform of harmonic space covariance with survey window effect. We will compare the both approach with the sample covariance measured from Gaussian realizations.

We organize this paper as follows. In Section 2, we summarize how to calculate the covariance of 2PCFs and power spectra analytically. In Section 3, we introduce Gaussian simulations of cosmic shear fields to measure the sample covariance with which we compare our analytical covariance estimation. In Section 4, we present the accuracy of analytic covariance estimate compared to the sample covariance. Section 5 is devoted to discussion and conclusion.

2 Formulation of the covariance matrix of cosmic shear two-point correlation function

2.1 Power spectrum with and without survey window effects

In this work, we consider the Gaussian covariance of weak gravitational lensing observables in a finite survey area. Specifically, we focus on the power spectrum, C_ℓ , of the spin-0 convergence field $\kappa(\hat{\mathbf{n}})$, defined on the celestial sphere. In practice, a survey is limited to a partial sky coverage and has complex geometry involved with masks. These affect the measured power spectrum and its covariance. We refer to this effect as the survey window effect and denote physical quantities affected by this effect with a tilde symbol, e.g., \tilde{C}_ℓ . We also consider the real-space counterpart of C_ℓ , the two-point correlation function $\xi(\theta)$. For simplicity, we restrict our analysis to a single source redshift.

On the celestial sphere, the convergence field κ in the direction $\hat{\mathbf{n}}$ is expanded in spherical harmonics $Y_{\ell m}$ as

$$\kappa(\hat{\mathbf{n}}) = \sum_{\ell, m} a_{\ell m} Y_{\ell m}(\hat{\mathbf{n}}), \quad (2.1)$$

and the power spectrum is defined by

$$\langle a_{\ell m} a_{\ell' m'}^* \rangle = \delta_{\ell\ell'}^K \delta_{mm'}^K C_\ell, \quad (2.2)$$

where $\delta_{\ell\ell'}^K$ is the Kronecker delta function.

The observed field including the survey window effect can be expressed as

$$\tilde{\kappa}(\hat{\mathbf{n}}) = w(\hat{\mathbf{n}})\kappa(\hat{\mathbf{n}}), \quad (2.3)$$

where $w(\hat{\mathbf{n}})$ is the survey mask field, defined as $w(\hat{\mathbf{n}}) = 1$ if $\hat{\mathbf{n}}$ lies inside the survey region, and $w(\hat{\mathbf{n}}) = 0$ otherwise. When weights are also taken into account, the following discussion can be straightforwardly extended. The resulting power spectrum can be expressed using the mode-coupling matrix $\mathcal{M}_{\ell\ell'}(w, w)$ [23, 26, 27] as

$$\tilde{C}_\ell = \sum_{\ell'} \mathcal{M}_{\ell\ell'}(w, w) C_{\ell'}. \quad (2.4)$$

From this equation, we can obtain the unwindowed (i.e., window-corrected) power spectrum via $C_\ell = \mathcal{M}_{\ell\ell'}^{-1} \tilde{C}_{\ell'}$. This is the so-called pseudo- C_ℓ method for estimating C_ℓ .

2.2 Relation between $\xi(\theta)$ and \tilde{C}_ℓ

The two-point correlation function of the convergence field is given by the Legendre transform of the power spectrum as

$$\xi(\theta) = \sum_{\ell} \frac{2\ell + 1}{4\pi} C_\ell P_\ell(\cos \theta), \quad (2.5)$$

where $P_\ell(x)$ is the Legendre polynomial.

The measured correlation function is an unbiased estimator of the underlying correlation function, in the sense that it is not affected by the survey window. Nevertheless, Ref. [14] derived the relation between the windowed (measured) power spectrum and the correlation function (see Appendix C of Ref. [14]):

$$\xi_i = \frac{n^2}{N_{\text{pair},i}} \tilde{\xi}_i, \quad (2.6)$$

where $\xi_i \equiv \xi[\theta_{i,-}, \theta_{i,+}]$ denotes the correlation function averaged over the i -th angular bin, n is the mean number density of source galaxies per steradian, and $N_{\text{pair},i}$ is the number of galaxy pairs in the i -th bin within the finite survey region. The quantity $\tilde{\xi}_i$ is the ‘‘window-affected’’ correlation function, defined in terms of the windowed power spectrum \tilde{C}_ℓ as

$$\tilde{\xi}_i = 2\pi \sum_{\ell} [P_{\ell+1}(x) - P_{\ell-1}(x)]_{\cos \theta_{i,+}}^{\cos \theta_{i,-}} \tilde{C}_\ell, \quad (2.7)$$

where we took average of $P_\ell(\cos \theta)$ over the angular bin using recursion relation of Legendre polynomials. Eq. (2.6) is non-trivial, and we will validate it using simulated maps of the weak lensing field.

2.3 Covariance matrix of $\xi(\theta)$

Following Appendix C of Ref. [14] and as indicated by Eqs. (2.6) and (2.7), the covariance matrix of the two-point correlation function can be *formally* expressed in terms of the covariance of \tilde{C}_ℓ as

$$\begin{aligned} \text{Cov}(\xi_i, \xi_j) &= \frac{n^4}{N_{\text{pair},i} N_{\text{pair},j}} \\ &\times (2\pi)^2 \sum_{\ell, \ell'} [P_{\ell+1}(x) - P_{\ell-1}(x)]_{\cos \theta_{i,+}}^{\cos \theta_{i,-}} [P_{\ell'+1}(x) - P_{\ell'-1}(x)]_{\cos \theta_{j,+}}^{\cos \theta_{j,-}} \times \text{Cov}(\tilde{C}_\ell, \tilde{C}_{\ell'}), \end{aligned} \quad (2.8)$$

where $\text{Cov}(\tilde{C}_\ell, \tilde{C}_{\ell'})$ is the covariance matrix of \tilde{C}_ℓ . As explicitly given by Eq. (C12) of [14], this is given in terms of the underlying power spectrum C_ℓ and the window function. Computing $\text{Cov}(\xi_i, \xi_j)$ directly requires $O(\ell_{\text{max}}^6)$ operations and is therefore computationally intractable, since we are interested in angular scales up to $\ell_{\text{max}} \sim \text{a few} \times O(10^3)$ (or even $O(10^4)$). For this reason, we need to adopt an approximation for $\text{Cov}(\tilde{C}_\ell, \tilde{C}_{\ell'})$ if we want to proceed with an analytical computation of $\text{Cov}(\xi_i, \xi_j)$, as proposed in Refs. [21–23].

2.3.1 Improved Narrow Kernel Approximation (iNKA)

In this paper, we adopt the improved Narrow Kernel Approximation (iNKA) [23] to calculate the covariance matrix $\text{Cov}(\tilde{C}_\ell, \tilde{C}_{\ell'})$ (see also [22] for the original NKA formalism). The iNKA assumes that the mode-coupling matrix is sharply localized around $\ell \simeq \ell'$, thereby enabling a fast computation of the Gaussian covariance of \tilde{C}_ℓ :

$$\text{Cov}(\tilde{C}_\ell, \tilde{C}_{\ell'})^{\text{iNKA}} = \frac{1}{2} \left(\frac{\tilde{C}_\ell + \tilde{C}_{\ell'}}{\langle w^2 \rangle_{\text{pixel}}} \right)^2 \Xi_{\ell\ell'}(w^2, w^2), \quad (2.9)$$

where $\langle \cdot \rangle_{\text{pix}}$ denotes the averaging the quantity inside brackets over all pixels, and the matrix $\Xi_{\ell\ell'}(w^2, w^2)$ is defined as

$$\Xi_{\ell\ell'}(w^2, w^2) \equiv \frac{\mathcal{M}_{\ell\ell'}(w^2, w^2)}{2\ell' + 1}. \quad (2.10)$$

Here $\mathcal{M}_{\ell\ell'}$ is the mode-coupling matrix defined in a similar way to $\mathcal{M}_{\ell\ell'}$ Eq. (2.4), but using the squared weight field w^2 instead of w in the calculation. The matrix $\Xi_{\ell\ell'}$ depends only on the weight field, and its computation is inexpensive when using a spherical harmonic expansion of the weight field.

By substituting this expression into the covariance formula of $\text{Cov}(\xi_i, \xi_j)$ (Eq. 2.8), one can perform the calculation efficiently. In this work, we assess the accuracy of this analytical approach by comparing its predictions with those computed from realizations of simulated lensing fields.

2.3.2 The f_{sky} approximation

The f_{sky} approximation is commonly used in previous studies to compute the covariance of cosmic shear fields [18]. The covariance of the power spectrum with the f_{sky} approximation is given by

$$\text{Cov}(C_\ell, C_{\ell'})^{f_{\text{sky}}} = \delta_{\ell\ell'}^K \frac{2C_\ell^2}{(2\ell + 1)f_{\text{sky}}}, \quad (2.11)$$

where f_{sky} is the sky fraction covered by the survey. The covariance of ξ can be computed by integrating the power spectrum covariance, weighted by Legendre polynomials, over the bin width:

$$\begin{aligned} \text{Cov}(\xi_i, \xi_j)^{f_{\text{sky}}} &= \sum_{\ell, \ell'} \frac{[P_{\ell+1}(x) - P_{\ell-1}(x)]_{\cos \theta_{i,+}}^{\cos \theta_{i,-}} [P_{\ell'+1}(x) - P_{\ell'-1}(x)]_{\cos \theta_{j,+}}^{\cos \theta_{j,-}}}{(4\pi)^2 (\cos \theta_{i,-} - \cos \theta_{i,+}) (\cos \theta_{j,-} - \cos \theta_{j,+})} \\ &\quad \times \text{Cov}(C_\ell, C_{\ell'})^{f_{\text{sky}}}. \end{aligned} \quad (2.12)$$

We will compare the covariance obtained with the f_{sky} approximation to those obtained from the simulations and the iNKA.

3 Gaussian simulations of cosmic shear fields

3.1 Cosmological parameters and simulation setups

To assess the accuracy of the analytical methods for computing the Gaussian covariance matrix of cosmic shear correlation functions, we use a large number of Gaussian realizations

of cosmic shear fields. In this subsection, we describe the method used to construct the Gaussian simulations.

First, we compute the input power spectrum of the convergence field for a fiducial flat Λ CDM model using the Core Cosmology Library (CCL) [28]. The flat Λ CDM model is specified by the following parameters: $\Omega_c = 0.233$ and $\Omega_b = 0.046$, the density parameters of CDM and baryon, respectively; $\sigma_8 = 0.82$ and $n_s = 0.97$, the normalization and spectral index of the linear power spectrum; and the Hubble parameter $h = 0.7$. We use HEALPix [29] to generate the convergence fields from the input power spectrum on the celestial sphere. Here we adopt a pixel resolution of $N_{\text{side}} = 2048$, corresponding to a pixel scale of approximately 1.7 arcmin. Then we apply the HSC Year 3 (HSC-Y3) survey mask [30] to obtain a masked map of the lensing fields. We use 1,000 realizations of the lensing fields for statistical analyses.

3.2 Measurements of \tilde{C}_ℓ , $\xi(\theta)$, and their covariance matrices from simulated maps

From each convergence map, we measure \tilde{C}_ℓ , which is affected by the survey window, using NaMaster [27]. We compute the mean and covariance over the realizations as follows:

$$\begin{aligned}\tilde{C}_\ell^{\text{sim}} &= \frac{1}{N_{\text{sim}}} \sum_{r=1}^{N_{\text{sim}}} \tilde{C}_\ell^{(r)}, \\ \text{Cov}(\tilde{C}_\ell, \tilde{C}_{\ell'})^{\text{sim}} &= \frac{1}{N_{\text{sim}} - 1} \sum_{r=1}^{N_{\text{sim}}} (\tilde{C}_\ell^{(r)} - \tilde{C}_\ell^{\text{sim}})(\tilde{C}_{\ell'}^{(r)} - \tilde{C}_{\ell'}^{\text{sim}}),\end{aligned}\quad (3.1)$$

where $N_{\text{sim}} = 1,000$, the number of the Gaussian realizations.

For each realization, we construct a convergence catalog by assigning to each galaxy position in the HSC-Y3 galaxy catalog the value of the convergence field at the corresponding position on the masked map pixel. We then measure the two-point correlation function from the resulting catalog using TreeCorr [31]. Repeating this procedure for all realizations, we estimate the mean and covariance over the realizations in the same manner as for the power spectrum:

$$\begin{aligned}\xi_i^{\text{sim}} &= \frac{1}{N_{\text{sim}}} \sum_{r=1}^{N_{\text{sim}}} \xi_i^{(r)} \\ \text{Cov}(\xi_i, \xi_j)^{\text{sim}} &= \frac{1}{N_{\text{sim}} - 1} \sum_{r=1}^{N_{\text{sim}}} (\xi_i^{(r)} - \xi_i^{\text{sim}})(\xi_j^{(r)} - \xi_j^{\text{sim}}).\end{aligned}\quad (3.2)$$

We employ 20 logarithmically-spaced bins in the range $\theta = [6, 300]$ arcmin.

4 Results

4.1 Signal of \tilde{C}_ℓ , $\xi(\theta)$

First, we validate the relation between ξ and $\tilde{\xi}$ (Eq. 2.6) which provides the basis for the following discussion on the covariance of ξ .

Fig. 1 shows the mean of the measured power spectrum, $\tilde{C}_\ell^{\text{sim}}$ (black points), the input theoretical power spectrum C_ℓ (blue line), and the window-convolved power spectrum \tilde{C}_ℓ obtained via the mode-coupling matrix (red line). We can see that the multiplication of the mode-coupling matrix (Eq. 2.4) captures the survey window effect accurately.

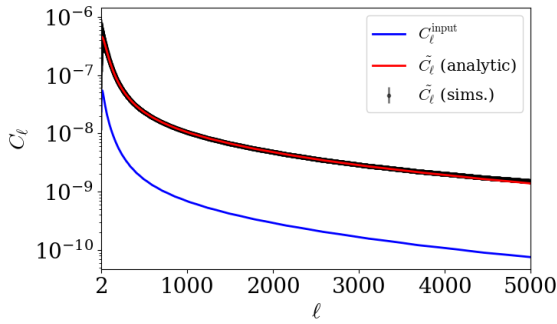


Figure 1. Input power spectrum C_ℓ (blue line), the window-convolved power spectrum \tilde{C}_ℓ obtained via the mode-coupling matrix (red line), and the mean power spectrum measured from Gaussian simulations (black points with error bars). The agreement demonstrates that the mode-coupling matrix accurately captures the survey window effect.

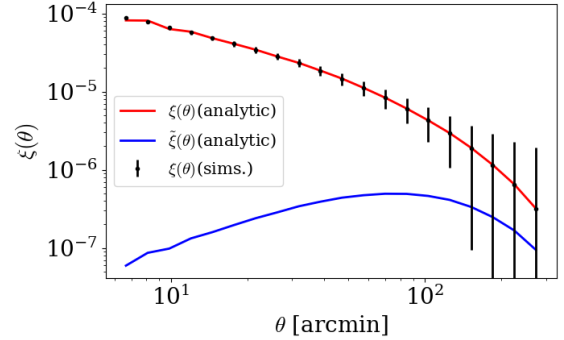


Figure 2. Mean of correlation function ξ^{sim} (black points with error bars). Error bars correspond to $\sqrt{\text{Cov}(\xi, \xi)^{\text{sim}}}$. Blue line shows $\tilde{\xi}$ calculated via Eq. 2.7. Red line shows ξ calculated via Eq. 2.6.

We can correct the window effect on correlation function by multiplying the corresponding θ -dependent factor as in Eq. 2.6. Fig. 2 shows the measured mean of correlation function ξ^{sim} (black points with errorbars). First, we calculate $\tilde{\xi}$ (blue line) using \tilde{C}_ℓ via Eq. 2.7. Then we obtain ξ (red line) using Eq. 2.6. We find good agreement between ξ (Eq. 2.6) and measured one.

4.2 Covariance of $\xi(\theta)$

First, we compare the analytically calculated covariance $\text{Cov}(\tilde{C}_\ell, \tilde{C}_{\ell'})$ based on iNKA with the covariance measured from the simulations, $\text{Cov}(\tilde{C}_\ell, \tilde{C}_{\ell'})^{\text{sim}}$. Fig. 3 shows that, for the diagonal components, we find good agreement between the two. The ratio between simulations and iNKA is consistent within 10%.

Fig. 4 shows diagonal components of $\text{Cov}(\xi_i, \xi_j)$, measured from Gaussian realizations (dashed line) and calculated using Eq. 2.8 (solid lines). In Eq. 2.8, we set $\ell_{\text{max}} = 3N_{\text{side}} - 1 = 6143$. The good agreement between projection of $\text{Cov}(\tilde{C}_\ell, \tilde{C}_{\ell'})$ measured from Gaussian simulations (blue) and $\text{Cov}(\xi_i, \xi_j)^{\text{sim}}$ indicates Eq. 2.8 is accurate and taking $\ell_{\text{max}} = 6143$ is enough to calculate the covariance accurately. On the other hand, projection of $\text{Cov}(\tilde{C}_\ell, \tilde{C}_{\ell'})$ calculated using iNKA (red) fails to reproduce $\text{Cov}(\xi_i, \xi_j)^{\text{sim}}$. A possible reason why $\text{Cov}(\xi_i, \xi_j)$ computed using $\text{Cov}(\tilde{C}_\ell, \tilde{C}_{\ell'})^{\text{iNKA}}$ does not agree with $\text{Cov}(\xi_i, \xi_j)^{\text{sim}}$, measured directly from Gaussian simulations, is the limited accuracy of the iNKA itself.

Fig. 5 compares the correlation matrices of $\text{Cov}(\tilde{C}_\ell, \tilde{C}_{\ell'})$ computed using the iNKA and measured from Gaussian simulations. The right panel shows the ratio between the two covariance estimates. Although the iNKA reproduces the diagonal structure accurately, visible discrepancies remain in the off-diagonal components. This behavior is consistent with the underlying assumption of iNKA. Specifically, the iNKA relies on the mode-coupling kernel being sharply localized around $\ell \simeq \ell'$. It is therefore effective for diagonal-dominated quantities, but its errors can be amplified in situations where off-diagonal information is required with high precision. Indeed, in the calculation of $\text{Cov}(\xi_i, \xi_j)$, the contribution from the off-

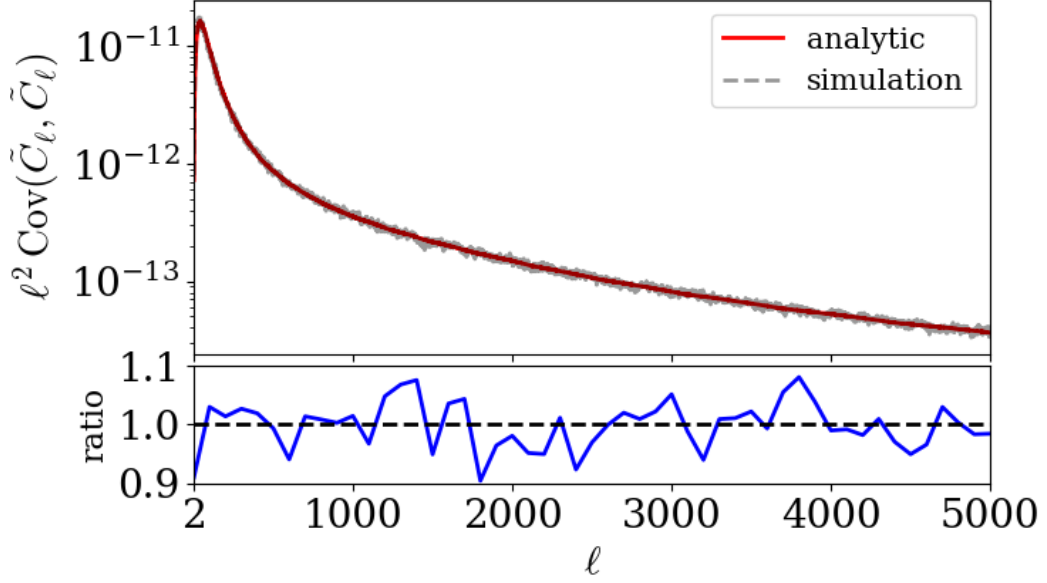


Figure 3. Upper panel: Diagonal components of $\text{Cov}(\tilde{C}_\ell, \tilde{C}_{\ell'})$, measured from 1000 Gaussian realizations (dashed line) and calculated using Eq. 2.9 (solid lines). Lower panel: Ratio of the analytical prediction based on the iNKA to the simulation results. The ratio is consistent within 10%.

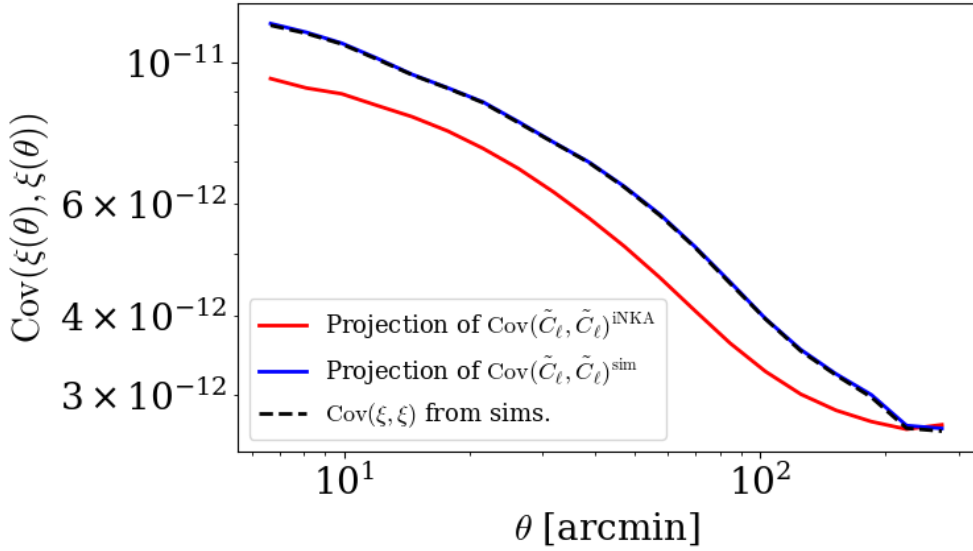


Figure 4. Diagonal components of $\text{Cov}(\xi[\theta_-, \theta_+], \xi[\theta'_-, \theta'_+])$, measured from Gaussian realizations (dashed line) and calculated using Eq. 2.8 (solid lines).

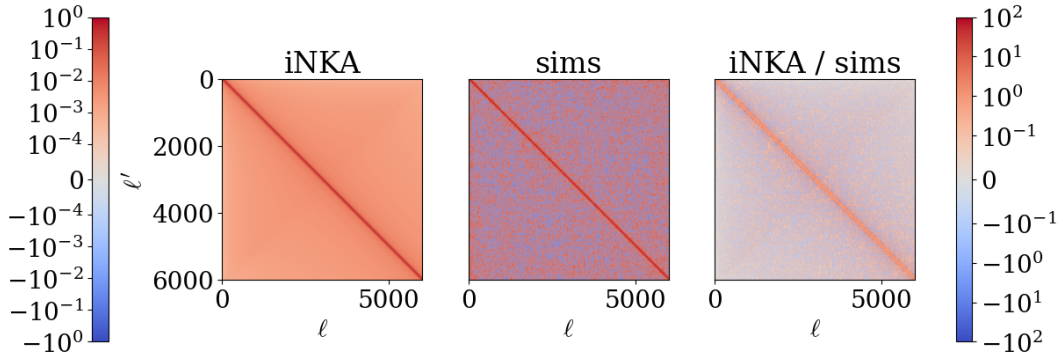


Figure 5. Correlation matrices of $\text{Cov}(\tilde{C}_\ell, \tilde{C}_{\ell'})$ computed using the iNKA (left) and measured from Gaussian simulations (center). The colors corresponding to the map values are depicted on the left. The right plot shows the ratio $\text{Cov}(\tilde{C}_\ell, \tilde{C}_{\ell'})^{\text{iNKA}} / \text{Cov}(\tilde{C}_\ell, \tilde{C}_{\ell'})^{\text{sim}}$ and color bar is shown on the right. The iNKA reproduces the diagonal structure accurately, while noticeable differences remain in the off-diagonal components.

diagonal components of $\text{Cov}(\tilde{C}_\ell, \tilde{C}_{\ell'})$ is not negligible as can be seen in Eq. 2.8. Therefore, if one computes $\text{Cov}(\xi_i, \xi_j)$ by simply extending the iNKA, the resulting accuracy will be degraded as shown in Fig. 4.

4.3 2PCF covariance from quartic counts

Alternatively, the 2PCFs covariance can be calculated as galaxy quartic counts weighted by $\xi \times \xi$ (and galaxy weights) [13, 25]:

$$\text{Cov}(\xi_i, \xi_j) = \frac{1}{N_{\text{pair},i} N_{\text{pair},j}} \sum_{a,b,c,d} w_a w_b w_c w_d \Delta_{\theta_i}(\theta_{ab}) \Delta_{\theta_j}(\theta_{cd}) \left\{ \xi(\theta_{ac}) \xi(\theta_{bd}) + \xi(\theta_{ad}) \xi(\theta_{bc}) \right\} / 2, \quad (4.1)$$

where w_a is the measurement weight for the a -th galaxy, θ_{ab} is angular separation between the a -th and b -th galaxies, and $\Delta_{\theta_i}(\theta_{ab})$ is 1 if $\theta_{i,-} < \theta_{ab} < \theta_{i,+}$ and 0 otherwise. We have neglected the terms involved with the shape noise. We derive the matrix expression of Eq (4.1) to make the calculation faster:

$$\text{Cov}(\xi_i, \xi_j) = \frac{1}{2N_{\text{pair},i} N_{\text{pair},j}} \sum_{\mu,\nu} [(\mathbf{w}_i \mathbf{w}_j^T) \odot (\mathbf{\Xi}_{1,i} \mathbf{\Xi}_{1,j}^T + \mathbf{\Xi}_{2,i} \mathbf{\Xi}_{2,j}^T)]_{\mu,\nu}. \quad (4.2)$$

The vector \mathbf{w}_i (\mathbf{w}_j) with the length $N_{\text{pair},i}$ ($N_{\text{pair},j}$) is defined by arranging the pair weights $w_a w_b$ ($w_c w_d$). The vector $\mathbf{\Xi}_{1,i}$ ($\mathbf{\Xi}_{1,j}$) with the length $N_{\text{pair},i}$ ($N_{\text{pair},j}$) is defined by arranging $\xi(\theta_{ac})$ ($\xi(\theta_{bd})$), and similarly for the other combinations. The symbol \odot denotes element-wise multiplication. We further merge galaxies into coarse grid ($N_{\text{side}} = 256$ or 512 depending on θ_i) to reduce the size of the matrices. In the following, we consider one of the six sub-fields in HSC-Y3, XMM field, and employ 10 logarithmically-spaced bins in the range $\theta = [6, 300]$ arcmin, to ease the computational expense.

Figure 6 compares the diagonal components of the covariance matrix computed using three analytical methods with those measured from Gaussian simulations. We find that the quartic counts method reproduces the simulation results more accurately than the approaches based on the iNKA and f_{sky} approximations.

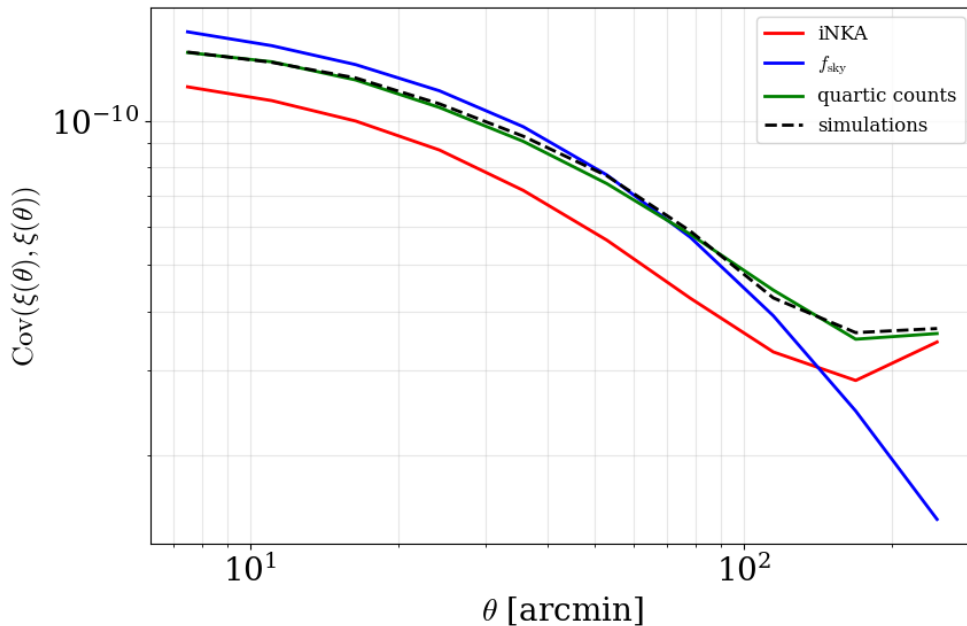


Figure 6. Diagonal components of $\text{Cov}(\xi[\theta_-, \theta_+], \xi[\theta'_-, \theta'_+])$, measured from Gaussian realizations (dashed line) and calculated using analytical methods (solid lines). Note that we consider XMM field only for this figure.

5 Conclusion

In this work, we have investigated analytical methods for computing the covariance matrix of the cosmic shear two-point correlation function, taking into account the effects of the survey window.

Our approach is based on constructing the covariance of the real-space correlation function $\xi(\theta)$ from the covariance of the windowed power spectrum \tilde{C}_ℓ , using the Legendre transformation. As a prerequisite, we have validated that the pseudo- C_ℓ framework correctly describes the impact of the survey window, and that the relation between $\tilde{\xi}$ and ξ (Eq. 2.6) provides an accurate mapping between harmonic and real space.

The main result of this study is that the covariance of $\xi(\theta)$ obtained by projecting the covariance of \tilde{C}_ℓ computed under the iNKA fails to reproduce the covariance measured from Gaussian simulations, even at the level of the diagonal components. This discrepancy arises because the iNKA, while it is accurate for the diagonal components of $\text{Cov}(\tilde{C}_\ell, \tilde{C}_{\ell'})$, does not adequately capture the off-diagonal structure. Since the computation of $\text{Cov}(\xi(\theta), \xi(\theta'))$ involves contributions from off-diagonal modes through the Legendre transformation, the inaccuracy propagates and leads to a degradation in the final covariance.

We have compared this approach with other analytical methods, including the f_{sky} approximation and the weighted quartic counts method proposed by Schneider et al. (2002) [25]. We find that the quartic counts method provides better agreement with the simulation results, highlighting the importance of accurately modeling pair-based correlations in configuration space.

Our results demonstrate that achieving an accurate prediction of the covariance matrix in real space requires precise modeling of mode coupling beyond diagonal approximations in

harmonic space. This has important implications for future wide-area surveys, where accurate covariance estimation is essential for cosmological parameter inference.

Acknowledgments

We thank LSST DESC MCPCov group for useful discussion. This work was supported in part by JSPS KAKENHI Grant Number 20H05600, 20H05855, 23KJ0747, 24H00215, and by World Premier International Research Center Initiative (WPI Initiative), MEXT, Japan.

References

- [1] M. Shirasaki, T. Hamana, M. Takada, R. Takahashi and H. Miyatake, *Mock galaxy shape catalogues in the Subaru Hyper Suprime-Cam Survey*, *Mon. Not. Roy. Astron. Soc.* **486** (2019) 52 [[1901.09488](#)].
- [2] X. Li, T. Zhang, S. Sugiyama, R. Dalal, R. Terasawa, M. M. Rau et al., *Hyper Suprime-Cam Year 3 results: Cosmology from cosmic shear two-point correlation functions*, *Phys. Rev. D* **108** (2023) 123518 [[2304.00702](#)].
- [3] R. Dalal, X. Li, A. Nicola, J. Zuntz, M. A. Strauss, S. Sugiyama et al., *Hyper Suprime-Cam Year 3 results: Cosmology from cosmic shear power spectra*, *Phys. Rev. D* **108** (2023) 123519 [[2304.00701](#)].
- [4] R. Terasawa, X. Li, M. Takada, T. Nishimichi, S. Tanaka, S. Sugiyama et al., *Exploring the baryonic effect signature in the Hyper Suprime-Cam Year 3 cosmic shear two-point correlations on small scales: The S8 tension remains present*, *Phys. Rev. D* **111** (2025) 063509 [[2403.20323](#)].
- [5] J. Ferri, E. G. M. Ferreira and R. Terasawa, *The contribution from small scales on two-point shear analysis: comparison between power spectrum and correlation function*, *arXiv e-prints* (2025) [arXiv:2512.17022](#) [[2512.17022](#)].
- [6] R. Takahashi, T. Hamana, M. Shirasaki, T. Namikawa, T. Nishimichi, K. Osato et al., *Full-sky gravitational lensing simulation for large-area galaxy surveys and cosmic microwave background experiments*, *The Astrophysical Journal* **850** (2017) 24.
- [7] M. Takada and W. Hu, *Power spectrum super-sample covariance*, *Phys. Rev. D* **87** (2013) 123504 [[1302.6994](#)].
- [8] R. Terasawa, R. Takahashi, T. Nishimichi and M. Takada, *Separate universe approach to evaluate nonlinear matter power spectrum for nonflat Λ CDM model*, *Phys. Rev. D* **106** (2022) 083504 [[2205.10339](#)].
- [9] R. Terasawa, R. Takahashi, T. Nishimichi and M. Takada, *Flat to nonflat: Calculating nonlinear power spectra of biased tracers for a nonflat Λ CDM model*, *Phys. Rev. D* **109** (2024) 063504 [[2310.13330](#)].
- [10] M. Sato, M. Takada, T. Hamana and T. Matsubara, *Simulations of Wide-field Weak-lensing Surveys. II. Covariance Matrix of Real-space Correlation Functions*, *Astrophys. J.* **734** (2011) 76 [[1009.2558](#)].
- [11] E. Krause and T. Eifler, *cosmolike - cosmological likelihood analyses for photometric galaxy surveys*, *Mon. Not. Roy. Astron. Soc.* **470** (2017) 2100 [[1601.05779](#)].
- [12] R. Reischke, S. Unruh, M. Asgari, A. Dvornik, H. Hildebrandt, B. Joachimi et al., *KiDS-Legacy: Covariance validation and the unified ONECOVARIANCE framework for projected large-scale structure observables*, *Astronomy & Astrophysics* **699** (2025) A124 [[2410.06962](#)].

- [13] M. Shirasaki, T. Hamana, M. Takada, R. Takahashi and H. Miyatake, *Mock galaxy shape catalogues in the Subaru Hyper Suprime-Cam Survey*, *Mon. Not. Roy. Astron. Soc.* **486** (2019) 52 [[1901.09488](#)].
- [14] O. Friedrich et al., *Dark energy survey year 3 results: Covariance modelling and its impact on parameter estimation and quality of fit*, [2012.08568](#).
- [15] O. Friedrich, S. Seitz, T. F. Eifler and D. Gruen, *Performance of internal covariance estimators for cosmic shear correlation functions*, *Mon. Not. Roy. Astron. Soc.* **456** (2016) 2662 [[1508.00895](#)].
- [16] B. Joachimi, P. Schneider and T. Eifler, *Analysis of two-point statistics of cosmic shear. III. Covariances of shear measures made easy*, *Astronomy & Astrophysics* **477** (2008) 43 [[0708.0387](#)].
- [17] J. Harnois-Déraps, A. Amon, A. Choi, V. Demchenko, C. Heymans, A. Kannawadi et al., *Cosmological simulations for combined-probe analyses: covariance and neighbour-exclusion bias*, *Mon. Not. Roy. Astron. Soc.* **481** (2018) 1337 [[1805.04511](#)].
- [18] X. Fang, T. Eifler and E. Krause, *2D-FFTLg: efficient computation of real-space covariance matrices for galaxy clustering and weak lensing*, *Mon. Not. Roy. Astron. Soc.* **497** (2020) 2699 [[2004.04833](#)].
- [19] O. Truttero, J. Zuntz, A. Pourtsidou and N. Robertson, *Baryon-free S_8 tension with Stage IV cosmic shear surveys*, *The Open Journal of Astrophysics* **8** (2025) 19 [[2410.18191](#)].
- [20] J. DeRose, N. Weaverdyck, M. White, S.-F. Chen, D. Schlegel and A. Slosar, *Stealing Weak Lensing Source Galaxy Samples against Systematics using Wide Field Spectroscopy*, *arXiv e-prints* (2026) [arXiv:2603.10113](#) [[2603.10113](#)].
- [21] G. Efstathiou, *Myths and truths concerning estimation of power spectra: the case for a hybrid estimator*, *Mon. Not. Roy. Astron. Soc.* **349** (2004) 603 [[astro-ph/0307515](#)].
- [22] C. García-García, D. Alonso and E. Bellini, *Disconnected pseudo- C_l covariances for projected large-scale structure data*, *JCAP* **2019** (2019) 043 [[1906.11765](#)].
- [23] A. Nicola, C. García-García, D. Alonso, J. Dunkley, P. G. Ferreira, A. Slosar et al., *Cosmic shear power spectra in practice*, *JCAP* **2021** (2021) 067 [[2010.09717](#)].
- [24] M. A. Troxel, E. Krause, C. Chang, T. F. Eifler, O. Friedrich, D. Gruen et al., *Survey geometry and the internal consistency of recent cosmic shear measurements*, *Mon. Not. Roy. Astron. Soc.* **479** (2018) 4998 [[1804.10663](#)].
- [25] P. Schneider, L. van Waerbeke, M. Kilbinger and Y. Mellier, *Analysis of two-point statistics of cosmic shear. I. Estimators and covariances*, *Astronomy & Astrophysics* **396** (2002) 1 [[astro-ph/0206182](#)].
- [26] C. Hikage, M. Takada, T. Hamana and D. Spergel, *Shear power spectrum reconstruction using the pseudo-spectrum method*, *Mon. Not. Roy. Astron. Soc.* **412** (2011) 65 [[1004.3542](#)].
- [27] D. Alonso, J. Sanchez, A. Slosar and LSST Dark Energy Science Collaboration, *A unified pseudo- C_ℓ framework*, *Mon. Not. Roy. Astron. Soc.* **484** (2019) 4127 [[1809.09603](#)].
- [28] N. E. Chisari, D. Alonso, E. Krause, C. D. Leonard, P. Bull, J. Neveu et al., *Core Cosmology Library: Precision Cosmological Predictions for LSST*, *Astrophys. J. Suppl.* **242** (2019) 2 [[1812.05995](#)].
- [29] K. M. Górski, E. Hivon, A. J. Banday, B. D. Wandelt, F. K. Hansen, M. Reinecke et al., *HEALPix: A Framework for High-Resolution Discretization and Fast Analysis of Data Distributed on the Sphere*, *Astrophys. J.* **622** (2005) 759 [[astro-ph/0409513](#)].
- [30] X. Li, H. Miyatake, W. Luo, S. More, M. Oguri, T. Hamana et al., *The three-year shear catalog*

of the Subaru Hyper Suprime-Cam SSP Survey, *Publ. Astron. Soc. Japan* **74** (2022) 421 [[2107.00136](#)].

- [31] M. Jarvis, G. Bernstein and B. Jain, *The skewness of the aperture mass statistic*, *Mon. Not. Roy. Astron. Soc.* **352** (2004) 338 [[astro-ph/0307393](#)].